

Learning Visual Proxy for Compositional Zero-Shot Learning

Shiyu Zhang¹, Cheng Yan¹, Yang Liu², Chenchen Jing², Lei Zhou³, Wenjun Wang¹

¹Tianjin University, Tianjin, China

²Zhejiang University, Zhejiang, China

³Hainan University, Hainan, China

Abstract

Compositional Zero-Shot Learning (CZSL) aims to recognize novel attribute-object compositions by leveraging knowledge from seen compositions. Existing methods align textual prototypes with visual features through Vision-Language Models (VLMs), but they face two key limitations: (1) modality gaps hinder the discrimination of semantically similar composition pairs, and (2) single-modal textual prototypes lack fine-grained visual cues, creating bottlenecks in VLM-based CZSL. In this paper, we introduce **Visual Proxy Learning**, a novel approach that facilitates the learning of distinct visual distributions, effectively reducing the modality gap and improving compositional generalization performance. Specifically, we initialize visual proxies for various attributes, objects, and their compositions using text representations. By optimizing the visual space, we capture fine-grained visual cues and guide the learning of more discriminative visual representations for attributes, objects and compositions. Furthermore, we propose an effective **Cross-Modal Joint Learning (CMJL)** strategy that imposes cross-modal constraints between the original text-image space and the fine-grained visual space. This approach not only boosts generalization for previously unseen composition pairs but also sharpens the discrimination of similar pairs, fostering more robust and precise learning. Extensive experiments demonstrate state-of-the-art performance in closed-world scenarios and competitive open-world results across four established CZSL benchmarks, validating the effectiveness of our approach in advancing compositional generalization.

1. Introduction

In human cognition, the ability to recombine existing concepts to form new ones is essential for quickly acquiring new knowledge, a skill known as compositional generalization. Similarly, in computer vision, this ability is crucial for advancing models' adaptability to novel situations, which has led to the development of Compositional Zero-

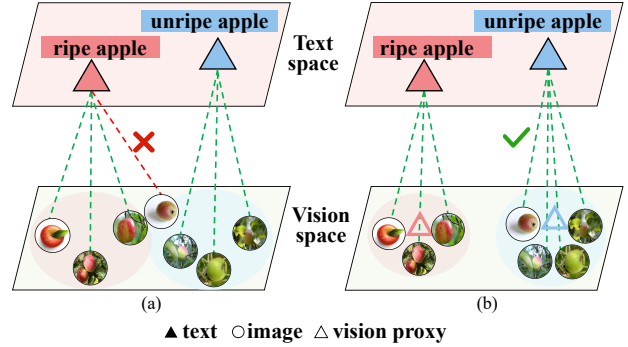


Figure 1. (a) The modality gap and coarse granularity of textual prototypes blur the inter-class boundaries in the visual space, causing classifiers to misclassify similar samples (e.g., slightly red unripe apples). (b) The visual proxy improves modality alignment, incorporates fine-grained image features, and makes the visual space more compact and separable, ensuring correct classification of similar samples.

Shot Learning (CZSL) [22, 27]. The goal of CZSL is to enable models to decompose and recombine concepts learned from seen compositions of attributes and objects, and then generalize to unseen compositions, thereby addressing the zero-shot image classification task. For instance, if a model is trained on compositions such as green clothes and red apples, it should be capable of recognizing novel compositions, like red clothes and green apples, during testing.

Thanks to the advancements in large pre-trained vision-language models like CLIP [31], recent research has made significant progress by leveraging CLIP and exploring various approaches to enhance its capabilities. These approaches include designing task-specific prompts [3, 17, 19, 26, 36, 37], decomposing compositional text features [18], and developing modal fusion methods [7] to narrow the modality gap. Such efforts have improved the alignment between compositional labels and image features, enabling CLIP to perform effectively in CZSL tasks. However, several challenges and inherent problems in the CZSL task still deserve attention.

Persistent Modality Gap. Despite efforts to narrow the modality gap between vision and language in existing

methods, it persists as a fundamental challenge in CZSL. While prior work [16] demonstrates that the gap can be partially reduced, complete elimination remains unattainable, particularly under the current task setup where classification depends critically on *top-1 cross-modal retrieval*. In such scenarios, the distance between true cross-modal pairs may exceed that of false pairs, leading to misclassifications directly attributable to the modality gap (see Fig. 1(a)). This problem is further amplified by the fine-grained nature of compositional semantics, where subtle visual distinctions—such as texture variations between “ripe” and “unripe” apples—are semantically critical yet notoriously difficult to align with their textual counterparts.

Limited Discriminability of Textual Prototypes. Existing VLM-based CZSL methods learn textual prototypes to address label scarcity, yet these prototypes inherently lack the fine-grained visual details crucial for distinguishing similar compositions. While each visual category contains diverse image instances (e.g., apples in varying shapes or lighting conditions), textual prototypes are derived from a single compositional label, resulting in a semantic-visual asymmetry. This mismatch prevents prototypes from capturing subtle distinctions (e.g., “ripe” vs. “unripe” apples), leading to ambiguous decision boundaries in the visual space (Fig. 1(a)). As shown in prior studies [29], relying solely on textual prototypes fails to approach the optimal performance for visual tasks.

Therefore, learning a class center in the visual modality is essential for CZSL. However, directly learning such centers is challenging due to the high variability of visual features (e.g., viewpoint and lighting variations), while the textual modality offers a more compact and semantically structured space. To overcome this challenge, we introduce the novel concept of **Visual Proxy** in CZSL, which leverages the well-established textual modality to guide the learning of visual centers. Building on this idea, we propose a **Cross-Modal Joint Learning (CMJL)** strategy that enables the collaborative optimization of textual prototypes and visual proxies, capitalizing on their complementary strengths while jointly facilitating composition pair recognition during the testing phase. This approach not only preserves the strong generalization capabilities of CLIP but also enhances discriminability in the visual space. In summary, our Visual Proxy-Based Cross-Modal Joint Learning (**VP-CMJL**) achieves two key objectives: (1) **Enhancing modality alignment:** By introducing visual proxies, semantic-level alignment from textual prototypes to the visual space can be achieved, alleviating semantic projection bias. (2) **Preserving Visual Granularity:** Visual proxies preserve fine-grained details through contrastive learning, enabling precise discrimination of visually similar categories, and making the visual feature space more compact and separable, as shown in Fig. 1(b).

Our main contributions are summarized as follows:

- **Visual Proxy.** We introduce a novel concept of visual proxy, the first to be applied in the CZSL task, as a learnable class center in the visual modality guided by the text modality. This concept not only enhances modality alignment but also captures fine-grained image features, improving the discrimination of similar compositions.
- **Cross-Modal Joint Learning.** We propose an effective Cross-Modal Joint Learning strategy that simultaneously optimizes textual prototypes and visual proxies through cross-modal constraints, leveraging the complementary strengths of both modalities to jointly predict compositions, while enhancing the model’s generalization and discriminative abilities.
- **Superior Performance on CZSL Benchmarks.** Extensive experiments on MIT-States, UT-Zappos, C-GQA and VAW-CZSL demonstrate state-of-the-art performance, validating the effectiveness of visual proxies and cross-modal joint learning.

2. Related Work

Compositional Zero-Shot Learning. Previous methods for CZSL can be categorized into two strategies: (1) Uniform feature representation learning, which establishes relationships between compositions and primitives (attributes and objects), embedding both images and compositions into a shared space for unseen composition prediction using a single classifier [1, 13, 21, 22, 24, 28]. (2) Multi-branch feature learning, which employs parallel discriminative modules for attributes, objects, and compositions, emphasizing visual feature discriminability [10, 12, 15, 25, 33, 34]. Recently, with the advancement of pre-trained Vision-Language Models (VLMs) and their strong generalization abilities, VLMs have been increasingly applied to CZSL [18, 19, 26, 36]. For instance, Nayak et al. [26] used soft prompts to treat attributes and objects as learnable tokens, while Xu et al. [37] constructed a graph[35] of object-attribute compositions. Lu et al. [18] decomposed states and objects in language features and integrated them with image features. Huang et al. [7] created three recognition branches to model attributes, objects, and compositions, aligning branch-specific prompt representations with visual features. Li et al. [14] proposed a context-based, diversity-driven specificity learning framework, considering attribute specificity levels.

Visual Center Learning. Previous work aims to obtain visual centers through prototypes by averaging image features within a single modality [13, 32]. However, such approaches face inherent limitations: (1) Prototypes derived solely from visual features are sensitive to viewpoint and lighting variations, leading to poor generalization; (2) Unimodal prototypes fail to capture fine-grained semantics of attribute-object compositions. To address these issues, we

propose the novel concept of Visual Proxy, which introduces textual modality as semantic guidance for the first time. Through cross-modal joint learning, Visual Proxy dynamically calibrates visual centers, achieving a balance between generalizability and discriminability.

3. Method

3.1. Problem Formulation

In CZSL, compositional labels consist of attributes and objects. Attributes are denoted as $a \in \mathcal{A}$, objects as $o \in \mathcal{O}$, and compositions as $c \in \mathcal{C}$, where $\mathcal{C} = \mathcal{A} \times \mathcal{O}$. The compositional label space is divided into seen compositions \mathcal{C}_s and unseen compositions \mathcal{C}_u , with $\mathcal{C}_s \cap \mathcal{C}_u = \emptyset$. The training set is defined as $\mathcal{T} = (x, c), |, x \in \mathcal{X}, c \in \mathcal{C}_s$, where \mathcal{X} represents the image space. During testing, the model must classify images from both seen and unseen compositions. CZSL can be categorized into closed-world and open-world settings based on the treatment of unseen compositions [20]. In the closed-world setting, unseen compositions \mathcal{C}_u are provided as prior knowledge, and the prediction space is $\mathcal{C}_{pred} = \mathcal{C}_s \cup \mathcal{C}_u$. In contrast, in the open-world setting, unseen compositions include all possible attribute-object compositions, and the prediction space is $\mathcal{C}_{pred} = \mathcal{A} \times \mathcal{O}$.

3.2. Basic Framework

To ensure generalization ability on unseen compositions, we follow previous works by utilizing frozen CLIP[31] and adapters[5] for feature extraction, and adopt the commonly effective three-path(attribute, object and composition) prediction framework [7, 14] in CZSL tasks.

Visual Representation. We leverage the CLIP image encoder E_v to extract the global image feature f_v^{cls} from the input image x , which serves as the image feature f_v^c for the composition branch. To achieve feature disentanglement, we employ two independent MLPs to process f_v^c , yielding the *attribute-oriented* image feature f_v^a and the *object-oriented* image feature f_v^o .

Prompt Representations. Following previous work, [7, 26, 39] we first construct the attribute prompt $\theta_i^a = [p_0^a, \dots, p_m^a, w_i^a]$, the object prompt $\theta_j^o = [p_0^o, \dots, p_m^o, w_j^o]$, and the composition prompt $\theta_{i,j}^c = [p_0^c, \dots, p_m^c, w_i^a, w_j^o]$. Here, $p_{0:m}^a$, $p_{0:m}^o$, and $p_{0:m}^c$ are prefixes initialized with the phrase “a photo of”, while w_i^a and w_j^o represent the vocabulary tokens for the attribute a_i and the object o_j , respectively. All components of the prompts are set as learnable parameters. Subsequently, we utilize the CLIP text encoder E_t to obtain the attribute text feature t_i^a , the object text feature t_j^o , and the composition text feature $t_{i,j}^c$.

Our Main Idea. Existing CZSL methods follow the CLIP classification paradigm through text-image matching, but the modality gap causes confusion between similar composition pairs, and relying solely on textual prototypes as class

labels lacks fine-grained features. To address these issues, we introduce text-guided visual proxies in the visual space and propose a Cross-Modal Joint Learning strategy, referred to as **VP-CMJL**, as shown in Fig. 2, which consists of the following two key innovative modules:

- **Text-Guided Visual Proxy Learning:** We introduce **visual proxies**—learnable centers in the visual space explicitly guided by textual semantics. Unlike traditional visual centers, visual proxies are dynamically optimized through cross-modal alignment, with text features serving as anchors to regularize the learning process. To enable better guidance of visual proxy learning by the text modality, we also design a corresponding textual prototype learning module, further enhancing modality alignment.
- **Cross-Modal Joint Learning:** During training, **CMJL** jointly optimizes visual proxies and textual prototypes using KL divergence, enabling the collaborative learning of both modalities. During inference, we compute and combine two compatibility scores: (1) between image features and textual prototypes for semantic alignment, and (2) between image features and visual proxies for fine-grained discrimination. The final prediction is a weighted fusion of these scores, dynamically balancing cross-modal consistency and visual specificity to enhance robustness.

3.3. Text-Guided Visual Proxy Learning

3.3.1. Textual Prototype Learning

The textual prototypes capture class-specific semantics at three levels (attributes, objects, compositions), following the multi-branch design in [7] to enhance generalization. For visual features, we introduce attribute cross-modal decoupling modules (**AD-CA**) and object cross-modal decoupling modules (**OD-CA**), aligning them with the corresponding textual prototypes to improve cross-modal consistency. Furthermore, we propose a novel probability calculation method that integrates attention scores.

The text representations are treated as textual prototypes, denoted as follows:

$$t^y = [t_1^y, t_2^y, \dots, t_{|\mathcal{Y}|}^y], \quad (1)$$

where $y \in \{a, o, c\}$, $|\mathcal{Y}| \in \{|\mathcal{A}|, |\mathcal{O}|, |\mathcal{C}_s|\}$. $|\mathcal{A}|$ and $|\mathcal{O}|$ denote the number of attributes and objects, respectively, $|\mathcal{C}_s|$ indicates the number of seen compositions during the training phase.

Cross-Modal Decoupling Module. Considering the gap between text and image, simple MLPs are insufficient for disentangling image features and aligning them with textual prototypes. To address this, we propose cross-modal decoupling modules, implemented as multi-head cross-attention [4], for the attribute and object branches, denoted as **AD-CA** and **OD-CA**. We focus on the attribute branch here,

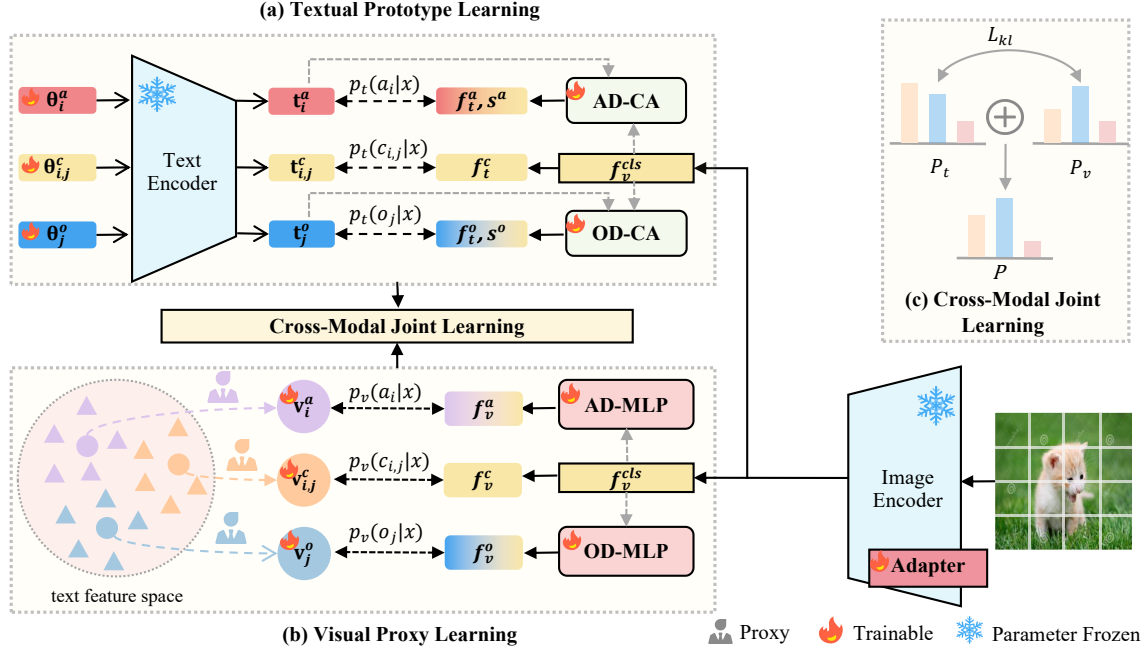


Figure 2. The overview of VP-CMJJ. (a) The Textual Prototype Learning Module utilizes a three-path framework and cross-modal image feature decoupling module to enhance semantic alignment between text and image. (b) The Visual Proxy Learning Module guides visual proxy learning using the text modality, aggregates hierarchical visual features, and preserves fine-grained discriminative information. (c) The Cross-Modal Joint Learning module employs a KL divergence constraint to collaboratively optimize textual prototypes and visual proxies. During the inference phase, both are combined to achieve composition pair prediction.

with the object branch following a similar process. Given the composition image feature $f_t^c = f_v^{cls} \in \mathbb{R}^d$ and attribute text prototypes $t^a \in \mathbb{R}^{|\mathcal{A}| \times d}$ as inputs, the query, key, and value are formulated as:

$$Q_a = f_t^c W_a^q, \quad K_a = t^a W_a^k, \quad V_a = t^a W_a^v, \quad (2)$$

where W_a^q , W_a^k , and $W_a^v \in \mathbb{R}^{d \times d_k}$ are the parameter matrices, with $d_k = d/h$, where h is the number of attention heads.

The attention score s^a between the image feature f_t^c and the attribute text prototype t^a is given by:

$$s^a = \frac{1}{h} \sum_{i=1}^h \text{softmax} \left(\frac{Q_{a,i} K_{a,i}^\top}{\sqrt{d/h}} \right). \quad (3)$$

The multi-head output is obtained by concatenating and linearly projecting:

$$O_a = \text{Concat}(s_1^a V_{a,1}, \dots, s_h^a V_{a,h}) W_a^o, \quad (4)$$

where $W_a^o \in \mathbb{R}^{d \times d}$ is the weight matrix.

The output O_a is then passed through a feed-forward network, followed by layer normalization and a residual connection to obtain the decoupled image feature f_t^a :

$$f_t^a = f_t^c + \text{FFN}_a(\text{LN}(f_t^c + O_a)). \quad (5)$$

After the **AD-CA** module, the attribute image feature f_t^a and attention score s^a are derived from the image feature f_t^c . Similarly, the object image feature f_t^o and attention score s^o can be obtained from **OD-CA**.

Attention Score-Based Probability Calculation. After obtaining the textual prototypes and image features for each branch, we calculate the probabilities for attributes, objects, and compositions. Unlike previous studies [7, 14], which treat the attribute and object branches separately, we account for the entanglement between attributes and objects in CZSL. For both the attribute and object branches, we incorporate the attention weights s^a and s^o between the original image features and textual prototypes into the traditional text-image similarity, enhancing the prediction of attributes and objects. The specific probability calculation is as follows:

The probability values of the Attribute and Object branches:

$$p_t(y_i|x) = \frac{\exp((f_t^y \cdot t_i^y + s_i^y)/\tau_t)}{\sum_{k=1}^{|\mathcal{Y}|} \exp((f_t^y \cdot t_k^y + s_k^y)/\tau_t)}, \quad (6)$$

where $y \in \{a, o\}$, $|\mathcal{Y}| \in \{|\mathcal{A}|, |\mathcal{O}|\}$, y_i represents the specific element in the set for each case (i.e., a_i and o_j).

The probability values of the Composition branch:

$$p_t(c_{i,j}|x) = \frac{\exp(f_t^c \cdot t_{i,j}^c / \tau_t)}{\sum_{k=1}^{|C_s|} \exp(f_t^c \cdot t_k^c / \tau_t)}, \quad (7)$$

where $\tau_t \in \mathbb{R}$ denotes the temperature parameter, which is pre-trained in CLIP. Subsequently, we compute the cross-entropy loss for each branch as follows:

$$\mathcal{L}_t^y = -\frac{1}{|\mathcal{X}|} \sum_{x \in \mathcal{X}} \log p_t(y|x), \quad (8)$$

where $y \in \{a, o, c\}$. Therefore, the total loss for the textual prototypes learning module \mathcal{L}_t is defined as:

$$\mathcal{L}_t = \gamma_{ao}(\mathcal{L}_t^a + \mathcal{L}_t^o) + \gamma_c \mathcal{L}_t^c. \quad (9)$$

The parameters γ_{ao} and γ_c are hyperparameters, and the analysis can be found in the supplementary materials.

3.3.2. Visual Proxy Learning

Why is the visual proxy needed? The textual prototype learning module described above is designed to narrow the gap between the visual and textual modalities, facilitating the learning of a unified class center. Previous studies [29] have demonstrated that the class center exists in the overlapping region between the visual and text spaces. As shown in Fig. 3 (a), \mathbf{z}_j is the class center of CLIP, which can be presented by two features from both modalities:

$$\mathbf{z}_j = \sqrt{a} \mathbf{z}_j^x + \sqrt{1-a} \mathbf{z}_j^\perp, \quad (10)$$

where \mathbf{z}_j^x is derived from the vision space and \mathbf{z}_j^\perp shows the component from the orthogonal subspace such that $\mathbf{z}_j^{x\top} \mathbf{z}_j^\perp = 0$, containing information unique to the textual modality. The class center \mathbf{z}_j in the intersection area embodies shared information from both modalities. However, due to the gap between these modalities, the class center in the overlapping region is still influenced by this discrepancy, which means the ideal state of Fig. 3(b) is almost impossible to reach. Given that the core of the CZSL task is image classification, the optimal solution for all class centers must lie within the vision space. Thus the balance of learning should be appropriately tilted toward visual modality. Considering that the visual center is difficult to obtain, we propose leveraging the text modality to guide its learning. To this end, we introduce visual proxy learning.

Visual Proxy Construction. To ensure the model’s generalization ability on unseen compositions, we introduce three-path visual proxy learning. We denote the attribute visual proxies as v^a and the object visual proxies as v^o , as follows:

$$v^a = [v_1^a, v_2^a, \dots, v_{|A|}^a], \quad v_i^a \in \mathbb{R}^{1 \times d} \quad (11)$$

$$v^o = [v_1^o, v_2^o, \dots, v_{|O|}^o], \quad v_j^o \in \mathbb{R}^{1 \times d} \quad (12)$$

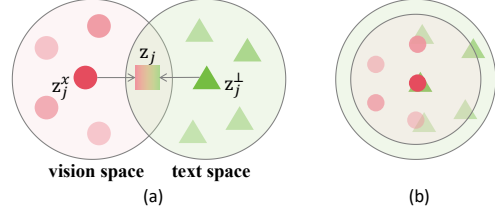


Figure 3. (a) Illustration of the visual and text spaces, where the class prototype \mathbf{z}_j resides in the overlapping region. (b) Ideal scenario where the visual space is fully covered by the text space.

where d represents the dimension of image features.

Given the inherent challenges of learning discriminative visual proxies via random initialization, which often leads to suboptimal local optima due to sparse training signals, we leverage the compact and semantically stable representations from pre-trained language models (PLMs). Specifically, we initialize visual proxies with text-derived embeddings:

$$v_i^a = E_l(w_i^a), \quad v_j^o = E_l(w_j^o), \quad (13)$$

where E_l denotes the text encoder of PLMs like BERT[11], GPT[30] or CLIP[31]. Importantly, our Appendix provides a comprehensive analysis of PLM selection for proxy initialization. The experiment shows that using CLIP’s text feature as initialization yields the best results.

Given that CZSL requires the classification of unseen compositions during testing, we set the attribute visual proxies, v^a , and the object visual proxies, v^o , as learnable parameters, and concatenate them to obtain the composition visual proxies, v^c :

$$v_{i,j}^c = E_c([v_i^a, v_j^o]), \quad (14)$$

where E_c is a fully connected layer that projects the concatenated composition proxies into the visual embedding space, ensuring consistency with the dimensionality of the image features.

MLP Decoupling Module. To decompose features in the visual modality for visual proxies learning, we replace the Cross-Modal Decoupling Module with an MLP Decoupling Module because it is an intra-modality learning process. As described in Sec. 3.2, for the attribute and object branches, the global image feature f_v^{cls} is processed through the **AD-MLP** and **OD-MLP** modules to obtain the attribute image feature f_v^a and object image feature f_v^o , while the composition image feature remains unchanged, i.e., $f_v^c = f_v^{cls}$.

Visual Proxies Training. To construct discriminative visual proxies, we optimize feature embeddings via intra-category attraction and inter-category repulsion, the specific probability calculations for each branch are outlined as follows:

$$p_v(y_{i,j}|x) = \frac{\exp(f_v^y \cdot v_{i,j}^y / \tau_v)}{\sum_{k=1}^{|Y|} \exp(f_v^y \cdot v_k^y / \tau_v)}, \quad (15)$$

where $y \in \{a, o, c\}$, $|\mathcal{Y}| \in \{|\mathcal{A}|, |\mathcal{O}|, |\mathcal{C}_s|\}$, $y_{i,j}$ represents the specific element in the set for each case (i.e., a_i , o_j , or $c_{i,j}$), τ_v is the temperature coefficient for the visual modality.

Subsequently, we calculate the cross-entropy loss for each branch:

$$\mathcal{L}_v^y = -\frac{1}{|\mathcal{X}|} \sum_{x \in \mathcal{X}} \log p_v(y|x), \quad (16)$$

where $y \in \{a, o, c\}$. This contrastive objective enforces image features to cluster tightly around their assigned proxies (intra-category compactness) while pushing away irrelevant proxies (inter-category separability).

Therefore, the total loss for the visual proxies learning module \mathcal{L}_v is defined as:

$$\mathcal{L}_v = \gamma_{ao}(\mathcal{L}_v^a + \mathcal{L}_v^o) + \gamma_c \mathcal{L}_v^c, \quad (17)$$

the analysis of the hyperparameters γ_{ao} and γ_c can be found in the supplementary material.

3.4. Cross-Modal Joint Learning

Training. To jointly learn optimal textual prototypes and visual proxies, we propose a KL divergence-based distribution alignment framework. Since the textual prototypes inherently capture semantically stable class representations through linguistic priors, while visual proxies trained from scratch are susceptible to training biases, we designate the textual prototypes as the target distribution and the visual proxies as the approximate distribution. The loss function is:

$$\mathcal{L}_{kl} = D_{KL}(P_t \| P_v) = \sum_x P_t(x) \log \frac{P_t(x)}{P_v(x)} \quad (18)$$

where P_t represents the probability distribution estimated by the textual prototypes, while P_v represents the probability distribution estimated by the visual proxies. Consequently, the total loss \mathcal{L} is expressed as follows:

$$\mathcal{L} = \alpha(\mathcal{L}_t + \mathcal{L}_v) + \beta \mathcal{L}_{kl}, \quad (19)$$

the analysis of the hyperparameters α and β can be found in the supplementary material.

By minimizing the loss function, we can obtain the optimal textual prototypes and visual proxies:

$$\mathbf{t}^*, \mathbf{v}^* = \arg \min_{\mathbf{t}, \mathbf{v}} (\mathcal{L}) \quad (20)$$

Inference. The trained textual and visual proxies are fused through multimodal probability aggregation. For each branch (attribute, object and composition), the final prediction probability is computed by:

$$p(y_{i,j}|x) = p_t(y_{i,j}|x) + \lambda p_v(y_{i,j}|x), \quad (21)$$

where $y \in \{a, o, c\}$, λ balances cross-modal contributions (empirically set to 1 for simplicity). The probability of the final prediction for a given sample is calculated as the sum of the attribute, object and composition probability:

$$p'(c_{i,j}|x) = p(c_{i,j}|x) + p(a_i|x) + p(o_j|x). \quad (22)$$

The final predicted composition is:

$$y' = \arg \max_{c_{i,j} \in \mathcal{C}_{pred}} (p'(c_{i,j}|x)) \quad (23)$$

4. Experiments

4.1. Experiments Setting

Datasets. We evaluated the model’s performance on four datasets: UT-Zappos [38], MIT-States [8], C-GQA [23], and VAW-CZSL[33]. The dataset information is shown in the supplementary material.

Metrics. Following standard open/closed-world settings [7, 14], we evaluate using Seen (S)/Unseen (U) composition accuracy, Harmonic Mean (HM), and Area Under Curve (AUC).

Implementation Details. To ensure fairness, we adopt the parameter settings established by previous research, utilizing the pre-trained CLIP ViT-L/14 model [31] as our image/text encoder. Training is conducted for 20 epochs in total. All training and testing are conducted on NVIDIA A800 GPUs. More details can be found in the supplementary material.

4.2. Main Results

We comprehensively evaluate our model under both closed-world and open-world settings, comparing it with recent CLIP-based CZSL methods from the past two years, including: CLIP[31], CoOp[39], CSP[26], DFSP[18], DLM[6], ProLT[9], PLID[3], CDS-CZSL[14], and Trokia[7]. The results are presented in Tab. 2. In the closed-world setting, our **VP-CMJL** achieves SOTA performance across all three datasets on nearly all metrics. Specifically, **VP-CMJL** improves the HM by +5.5%, +3.9%, and +1.1%, and the AUC by +3.9%, +6.2%, and +1.2%, respectively, across the three datasets, demonstrating the effectiveness of the proposed method. In the open-world setting, **VP-CMJL** significantly outperforms competing methods on the UT-Zappos and C-GQA datasets, with HM improvements of +6.7% and +4.6%, and AUC improvements of +8.4% and +1.9%, respectively. For the MIT-States dataset containing substantial label noise [2], the baseline method CDS-CZSL adopts dedicated pruning techniques specifically designed for open-world settings. Our method achieves competitive performance without relying on these task-specific optimizations.

Beyond standard benchmarks, we conduct a comprehensive evaluation on VAW-CZSL, a new large-scale real-world attribute dataset. While most existing methods lack

Table 1. The experimental results for both closed/open-world settings. The best performance are highlighted in bold.

| Method | Venue | C-GQA | | | | UT-Zappos | | | | MIT-States | | | |
|----------------------|---------|-------------|-------------|-------------|-------------|-------------|-------------|-------------|-------------|-------------|-------------|-------------|-------------|
| | | S | U | HM | AUC | S | U | HM | AUC | S | U | HM | AUC |
| Closed-world Results | | | | | | | | | | | | | |
| CLIP[31] | ICML'21 | 7.5 | 25.0 | 8.6 | 1.4 | 15.8 | 49.1 | 15.6 | 5.0 | 30.2 | 46.0 | 26.1 | 11.0 |
| CoOp[39] | IJCV'22 | 20.5 | 26.8 | 17.1 | 4.4 | 52.1 | 49.3 | 34.6 | 18.8 | 34.4 | 47.6 | 29.8 | 13.5 |
| CSP[26] | ICLR'23 | 28.8 | 26.8 | 20.5 | 6.2 | 64.2 | 66.2 | 46.6 | 33.0 | 46.6 | 49.9 | 36.3 | 19.4 |
| DFSP(i2t)[18] | CVPR'23 | 35.6 | 29.3 | 24.3 | 8.7 | 64.2 | 66.4 | 45.1 | 32.1 | 47.4 | 52.4 | 37.2 | 20.7 |
| DFSP(BiF)[18] | CVPR'23 | 36.5 | 32.0 | 26.2 | 9.9 | 63.3 | 69.2 | 47.1 | 33.5 | 47.1 | 52.8 | 37.7 | 20.8 |
| DFSP(t2i)[18] | CVPR'23 | 38.2 | 32.0 | 27.1 | 10.5 | 66.7 | 71.7 | 47.2 | 36.0 | 46.9 | 52.0 | 37.3 | 20.6 |
| DLM[6] | AAAI'24 | 32.4 | 28.5 | 21.9 | 7.3 | 67.1 | 72.5 | 52.0 | 39.6 | 46.3 | 49.8 | 37.4 | 20.0 |
| ProLT[9] | AAAI'24 | 39.5 | 32.9 | 27.7 | 11.0 | 66.0 | 70.1 | 49.4 | 36.1 | 49.1 | 51.0 | 38.2 | 21.1 |
| PLID[3] | ECCV'24 | 38.8 | 33.0 | 27.9 | 11.0 | 67.3 | 68.8 | 52.4 | 38.7 | 49.7 | 52.4 | 39.0 | 22.1 |
| CDS-CZSL[14] | CVPR'24 | 38.3 | 34.2 | 28.1 | 11.1 | 63.9 | 74.8 | 52.7 | 39.5 | 50.3 | 52.9 | 39.2 | 22.4 |
| Troika[7] | CVPR'24 | 41.0 | 35.7 | 29.4 | 12.4 | 66.8 | 73.8 | 54.6 | 41.7 | 49.0 | 53.0 | 39.3 | 22.1 |
| VP-CMJL(Ours) | | 46.0 | 40.2 | 34.9 | 16.3 | 71.9 | 76.3 | 58.5 | 47.9 | 51.8 | 52.6 | 40.4 | 23.3 |
| Open-world Results | | | | | | | | | | | | | |
| CLIP[31] | ICML'21 | 7.5 | 4.6 | 4.0 | 0.3 | 15.7 | 20.6 | 11.2 | 2.2 | 30.1 | 14.3 | 12.8 | 3.0 |
| CoOp[39] | IJCV'22 | 21.0 | 4.6 | 5.5 | 0.7 | 52.1 | 31.5 | 28.9 | 13.2 | 34.6 | 9.3 | 12.3 | 2.8 |
| CSP[26] | ICLR'23 | 28.7 | 5.2 | 6.9 | 1.2 | 64.1 | 44.1 | 38.9 | 22.7 | 46.3 | 15.7 | 17.4 | 5.7 |
| DFSP(i2t)[18] | CVPR'23 | 35.6 | 5.6 | 9.0 | 1.9 | 64.3 | 53.8 | 41.2 | 26.4 | 47.2 | 18.2 | 19.1 | 6.7 |
| DFSP(BiF)[18] | CVPR'23 | 36.5 | 7.6 | 10.6 | 2.4 | 63.5 | 57.2 | 42.7 | 27.6 | 47.1 | 18.1 | 19.2 | 6.7 |
| DFSP(t2i)[18] | CVPR'23 | 38.2 | 7.2 | 10.4 | 2.4 | 66.8 | 60.0 | 44.0 | 30.3 | 47.5 | 18.5 | 19.3 | 6.8 |
| PLID[3] | ECCV'24 | 39.1 | 7.5 | 10.6 | 2.5 | 67.6 | 55.5 | 46.6 | 30.8 | 49.1 | 18.7 | 20.4 | 7.3 |
| CDS-CZSL[14] | CVPR'24 | 37.6 | 8.2 | 11.6 | 2.7 | 64.7 | 61.3 | 48.2 | 32.3 | 49.4 | 21.8 | 22.1 | 8.5 |
| Troika[7] | CVPR'24 | 40.8 | 7.9 | 10.9 | 2.7 | 66.4 | 61.2 | 47.8 | 33.0 | 48.8 | 18.4 | 20.1 | 7.2 |
| VP-CMJL(Ours) | | 46.0 | 11.5 | 15.5 | 4.6 | 71.9 | 66.6 | 54.5 | 41.4 | 51.8 | 19.9 | 22.0 | 8.3 |

Table 2. The experimental results for the closed-world setting on the VAW-CZSL dataset. The best performance is highlighted in bold.

| Method | Venue | VAW-CZSL | | | |
|----------------------|---------|-------------|-------------|-------------|-------------|
| | | S | U | HM | AUC |
| CLIP[31] | ICML'21 | 23.9 | 18.0 | 11.9 | 2.6 |
| CSP[26] | ICLR'23 | 31.9 | 33.6 | 23.3 | 8.5 |
| DFSP[18] | CVPR'23 | 40.1 | 40.9 | 31.1 | 14.1 |
| CAILA[18] | WACV'24 | 41.6 | 49.2 | 34.6 | 17.2 |
| VP-CMJL(Ours) | | 47.8 | 51.1 | 38.2 | 20.7 |

Table 3. Results of ablation experiments on dual-modal center learning. 'TP'/'VP' represents the text prototypes and visual proxies.

| | | UT-Zappos | | | | MIT-States | | | |
|------------------------|----|-------------|-------------|-------------|-------------|-------------|-------------|-------------|-------------|
| TP | VP | S | U | HM | AUC | S | U | HM | AUC |
| Training and inference | | | | | | | | | |
| ✓ | ✓ | 71.9 | 76.3 | 58.5 | 47.9 | 51.8 | 52.6 | 40.4 | 23.3 |
| ✓ | ✗ | 64.4 | 70.7 | 51.9 | 37.8 | 47.1 | 52.1 | 37.8 | 20.8 |
| ✗ | ✓ | 65.8 | 72.3 | 55.3 | 42.1 | 50.5 | 49.4 | 37.6 | 20.7 |
| Inference | | | | | | | | | |
| ✓ | ✓ | 71.9 | 76.3 | 58.5 | 47.9 | 51.8 | 52.6 | 40.4 | 23.3 |
| ✓ | ✗ | 69.2 | 75.1 | 56.7 | 44.2 | 51.3 | 52.3 | 40.4 | 23.0 |
| ✗ | ✓ | 69.5 | 76.4 | 57.8 | 46.4 | 48.7 | 50.6 | 37.3 | 20.4 |

validation on this challenging benchmarks. As shown in Sec. 4.1, our approach improves the HM by +3.6% and AUC +3.5%, demonstrating the generalization ability and effectiveness of our model.

4.3. Ablation Study

Ablation study on VP-CMJL. To validate the effectiveness of visual proxies and cross-modal joint learning, we conduct ablation experiments in a closed-world setting on the UT-Zappos and MIT-States datasets. The experimental setup is as follows: (1) **Component removal:** Remove either the textual prototype (TP) or visual proxy (VP) during training and inference; (2) **Single-modal removal during inference:** Remove TP/VP only during testing, while maintaining full dual-modal training. The results (Tab. 3) show: (1) **Component necessity:** Removing either component causes a significant performance drop, confirming that the introduction of visual proxies benefits the CZSL task and must be learned in conjunction with textual prototypes, enhancing both CLIP's generalization and fine-grained discrimination capabilities. (2) **Training-testing dynamic difference:** The performance degradation is smaller when removing a modality during testing than during training, indicating that joint optimization promotes a synergistic representation enhancement mechanism during training.

Ablation study on decoupling modules. We exchange the decoupling modules on both modality. As shown in Tab. 4, the CA-/MLP-based decoupling module achieves the best effect for textual prototypes and visual proxies learning respectively. The results confirm that cross-modal decomposition aids in modality alignment, while MLP-based transformation is more effective for intra-modal learning.



Figure 4. Qualitative results. The term ‘w/o VP’ refers to the text-prototype-based method, while the green font indicates correct labels and the red font indicates incorrect labels.

Table 4. Results of ablation experiments on the decomposition modules. i2t/i2v represents the image feature decoupling method used in textual prototype/visual proxy learning, respectively.

| | | UT-Zappos | | | | MIT-States | | | |
|-----|-----|-------------|-------------|-------------|-------------|-------------|-------------|-------------|-------------|
| i2t | i2v | S | U | HM | AUC | S | U | HM | AUC |
| CA | MLP | 71.9 | 76.3 | 58.5 | 47.9 | 51.8 | 52.6 | 40.4 | 23.3 |
| CA | CA | 67.1 | 75.2 | 54.7 | 42.0 | 50.9 | 51.6 | 39.6 | 22.3 |
| MLP | CA | 67.3 | 76.2 | 55.7 | 44.2 | 50.8 | 52.5 | 39.6 | 22.8 |
| MLP | MLP | 69.5 | 73.1 | 58.5 | 45.3 | 50.0 | 51.4 | 38.8 | 21.8 |

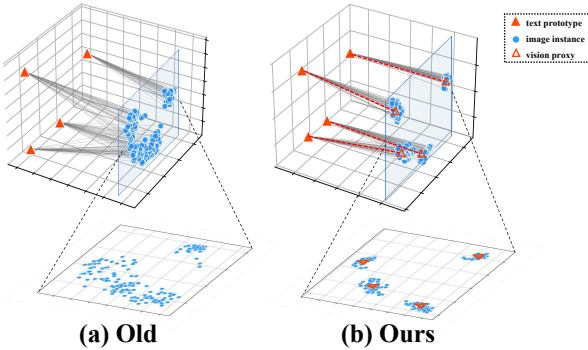


Figure 5. (a) Example of modality space feature distribution in traditional three-path methods. (b) Example of modality space feature distribution in **VP-CMJL**.

4.4. Quality Analysis

Case analysis. We visualize the qualitative results of the model on the C-GQA and MIT-States datasets in Fig. 4, showcasing both successful and failure cases for the proposed **VP-CMJL** model, as well as the text-prototype-based method (‘w/o VP’). The results clearly show that **VP-CMJL** effectively distinguishes between similar compositions, such as “large painting” vs. “large picture” or “broken bottle” vs. “spilled bottle,” while the text-prototype-based method struggles with compositions that have similar visual appearances. This demonstrates **VP-CMJL**’s ability

to learn fine-grained composition features. In failure cases, although the model often misclassifies the composition, it typically correctly identifies one of the primitives. Misclassifications are generally due to semantic similarity to the true label or some ambiguity.

Visualization of modality space features. As shown in Fig. 5, the comparison of modality feature spaces between the traditional three-path method and the proposed **VP-CMJL** framework highlights key differences. The baseline method suffers from rigid matching between textual prototypes and image features, resulting in cross-modal similarity measurement bias and a dispersed visual feature space with overlapping class boundaries. In contrast, **VP-CMJL** introduces a learnable visual proxy and bidirectional cross-modal adjustment, achieving semantic alignment and dynamically adjusting the mapping from image features to textual prototypes, leading to a more compact visual feature space and better class separability.

5. Conclusion

This work introduces the Visual Proxy and Cross-Modal Joint Learning strategy to address the challenges of Compositional Zero-Shot Learning (CZSL). By tackling the modality gap and the lack of fine-grained features, our approach introduces visual proxies for the first time and proposes a cross-modal joint learning strategy that enhances modality alignment and improves the discrimination of similar compositions, boosting generalization in CZSL tasks. Extensive experiments demonstrate that **VP-CMJL** outperforms existing methods in both closed-world and open-world settings, achieving state-of-the-art results. This work presents a promising direction for enhancing the generalization and discriminative power of compositional zero-shot learning by combining the strengths of textual and visual modalities.

References

- [1] Muhammad Umer Anwaar, Zhihui Pan, and Martin Kleinstreuber. On leveraging variational graph embeddings for open world compositional zero-shot learning. In *Proceedings of the 30th ACM International Conference on Multimedia*, pages 4645–4654, 2022. 2
- [2] Yuval Atzmon, Felix Kreuk, Uri Shalit, and Gal Chechik. A causal view of compositional zero-shot recognition. *Advances in Neural Information Processing Systems*, 33:1462–1473, 2020. 6
- [3] Wentao Bao, Lichang Chen, Heng Huang, and Yu Kong. Prompting language-informed distribution for compositional zero-shot learning. In *Proceedings of the European Conference on Computer Vision (ECCV)*, 2024. 1, 6, 7
- [4] Chun-Fu Richard Chen, Quanfu Fan, and Rameswar Panda. Crossvit: Cross-attention multi-scale vision transformer for image classification. In *Proceedings of the IEEE/CVF international conference on computer vision*, pages 357–366, 2021. 3
- [5] Shoufa Chen, Chongjian Ge, Zhan Tong, Jiangliu Wang, Yibing Song, Jue Wang, and Ping Luo. Adaptformer: Adapting vision transformers for scalable visual recognition. *Advances in Neural Information Processing Systems*, 35:16664–16678, 2022. 3
- [6] Xiaoming Hu and Zilei Wang. A dynamic learning method towards realistic compositional zero-shot learning. In *Proceedings of the AAAI Conference on Artificial Intelligence*, pages 2265–2273, 2024. 6, 7
- [7] Siteng Huang, Biao Gong, Yutong Feng, Min Zhang, Yiliang Lv, and Donglin Wang. Troika: Multi-path cross-modal traction for compositional zero-shot learning. In *Proceedings of the IEEE/CVF Conference on Computer Vision and Pattern Recognition*, pages 24005–24014, 2024. 1, 2, 3, 4, 6, 7
- [8] Phillip Isola, Joseph J Lim, and Edward H Adelson. Discovering states and transformations in image collections. In *Proceedings of the IEEE conference on computer vision and pattern recognition*, pages 1383–1391, 2015. 6
- [9] Chenyi Jiang and Haofeng Zhang. Revealing the proximate long-tail distribution in compositional zero-shot learning. In *Proceedings of the AAAI Conference on Artificial Intelligence*, pages 2498–2506, 2024. 6, 7
- [10] Shyamgopal Karthik, Massimiliano Mancini, and Zeynep Akata. Kg-sp: Knowledge guided simple primitives for open world compositional zero-shot learning. In *Proceedings of the IEEE/CVF Conference on Computer Vision and Pattern Recognition*, pages 9336–9345, 2022. 2
- [11] Jacob Devlin Ming-Wei Chang Kenton and Lee Kristina Toutanova. Bert: Pre-training of deep bidirectional transformers for language understanding. In *Proceedings of naacL-HLT*, page 2. Minneapolis, Minnesota, 2019. 5
- [12] Hanjae Kim, Jiyoung Lee, Seongheon Park, and Kwanghoon Sohn. Hierarchical visual primitive experts for compositional zero-shot learning. In *Proceedings of the IEEE/CVF International Conference on Computer Vision*, pages 5675–5685, 2023. 2
- [13] Xiangyu Li, Xu Yang, Kun Wei, Cheng Deng, and Muli Yang. Siamese contrastive embedding network for compositional zero-shot learning. In *Proceedings of the IEEE/CVF conference on computer vision and pattern recognition*, pages 9326–9335, 2022. 2
- [14] Yun Li, Zhe Liu, Hang Chen, and Lina Yao. Context-based and diversity-driven specificity in compositional zero-shot learning. In *Proceedings of the IEEE/CVF Conference on Computer Vision and Pattern Recognition*, pages 17037–17046, 2024. 2, 3, 4, 6, 7
- [15] Yong-Lu Li, Yue Xu, Xiaohan Mao, and Cewu Lu. Symmetry and group in attribute-object compositions. In *Proceedings of the IEEE/CVF conference on computer vision and pattern recognition*, pages 11316–11325, 2020. 2
- [16] Victor Weixin Liang, Yuhui Zhang, Yongchan Kwon, Serena Yeung, and James Y Zou. Mind the gap: Understanding the modality gap in multi-modal contrastive representation learning. *Advances in Neural Information Processing Systems*, 35:17612–17625, 2022. 2
- [17] Yang Liu, Xinlong Wang, Muzhi Zhu, Yue Cao, Tiejun Huang, and Chunhua Shen. Masked channel modeling for bootstrapping visual pre-training. *International Journal of Computer Vision*, pages 1–21, 2024. 1
- [18] Xiaocheng Lu, Song Guo, Ziming Liu, and Jingcai Guo. Decomposed soft prompt guided fusion enhancing for compositional zero-shot learning. In *Proceedings of the IEEE/CVF Conference on Computer Vision and Pattern Recognition*, pages 23560–23569, 2023. 1, 2, 6, 7
- [19] Xiaocheng Lu, Ziming Liu, Song Guo, Jingcai Guo, Fushuo Huo, Sikai Bai, and Tao Han. Drpt: Disentangled and recurrent prompt tuning for compositional zero-shot learning. *arXiv preprint arXiv:2305.01239*, 2023. 1, 2
- [20] Massimiliano Mancini, Muhammad Ferjad Naeem, Yongqin Xian, and Zeynep Akata. Open world compositional zero-shot learning. In *Proceedings of the IEEE/CVF conference on computer vision and pattern recognition*, pages 5222–5230, 2021. 3
- [21] Massimiliano Mancini, Muhammad Ferjad Naeem, Yongqin Xian, and Zeynep Akata. Learning graph embeddings for open world compositional zero-shot learning. *IEEE Transactions on pattern analysis and machine intelligence*, 46(3): 1545–1560, 2022. 2
- [22] Ishan Misra, Abhinav Gupta, and Martial Hebert. From red wine to red tomato: Composition with context. In *Proceedings of the IEEE Conference on Computer Vision and Pattern Recognition*, pages 1792–1801, 2017. 1, 2
- [23] Muhammad Ferjad Naeem, Yongqin Xian, Federico Tomba, and Zeynep Akata. Learning graph embeddings for compositional zero-shot learning. In *Proceedings of the IEEE/CVF Conference on Computer Vision and Pattern Recognition*, pages 953–962, 2021. 6
- [24] Muhammad Ferjad Naeem, Yongqin Xian, Federico Tomba, and Zeynep Akata. Learning graph embeddings for compositional zero-shot learning. In *Proceedings of the IEEE/CVF Conference on Computer Vision and Pattern Recognition*, pages 953–962, 2021. 2
- [25] Tushar Nagarajan and Kristen Grauman. Attributes as operators: factorizing unseen attribute-object compositions. In *Proceedings of the European Conference on Computer Vision (ECCV)*, pages 169–185, 2018. 2

- [26] Peilin Yu Nihal V. Nayak and Stephen H. Bach. Learning to compose soft prompts for compositional zero-shot learning. In *Proceedings of the International Conference on Learning Representations*, 2023. [1](#), [2](#), [3](#), [6](#), [7](#)
- [27] Senthil Purushwalkam, Maximilian Nickel, Abhinav Gupta, and Marc’Aurelio Ranzato. Task-driven modular networks for zero-shot compositional learning. In *Proceedings of the IEEE/CVF International Conference on Computer Vision*, pages 3593–3602, 2019. [1](#)
- [28] Senthil Purushwalkam, Maximilian Nickel, Abhinav Gupta, and Marc’Aurelio Ranzato. Task-driven modular networks for zero-shot compositional learning. In *Proceedings of the IEEE/CVF International Conference on Computer Vision*, pages 3593–3602, 2019. [2](#)
- [29] Qi Qian, Yuanhong Xu, and Juhua Hu. Intra-modal proxy learning for zero-shot visual categorization with clip. *Advances in Neural Information Processing Systems*, 36, 2024. [2](#), [5](#)
- [30] Alec Radford, Jeffrey Wu, Rewon Child, David Luan, Dario Amodei, Ilya Sutskever, et al. Language models are unsupervised multitask learners. *OpenAI blog*, 1(8):9, 2019. [5](#)
- [31] Alec Radford, Jong Wook Kim, Chris Hallacy, Aditya Ramesh, Gabriel Goh, Sandhini Agarwal, Girish Sastry, Amanda Askell, Pamela Mishkin, Jack Clark, et al. Learning transferable visual models from natural language supervision. In *International conference on machine learning*, pages 8748–8763, 2021. [1](#), [3](#), [5](#), [6](#), [7](#)
- [32] Frank Ruis, Gertjan Burghouts, and Doina Bucur. Independent prototype propagation for zero-shot compositionality. *Advances in Neural Information Processing Systems*, 34: 10641–10653, 2021. [2](#)
- [33] Nirat Saini, Khoi Pham, and Abhinav Shrivastava. Disentangling visual embeddings for attributes and objects. In *Proceedings of the IEEE/CVF Conference on Computer Vision and Pattern Recognition*, pages 13658–13667, 2022. [2](#), [6](#)
- [34] Qingsheng Wang, Lingqiao Liu, Chenchen Jing, Hao Chen, Guoqiang Liang, Peng Wang, and Chunhua Shen. Learning conditional attributes for compositional zero-shot learning. In *Proceedings of the IEEE/CVF Conference on Computer Vision and Pattern Recognition*, pages 11197–11206, 2023. [2](#)
- [35] Zengyi Wo, Minglai Shao, Wenjun Wang, Xuan Guo, and Lu Lin. Graph contrastive learning via interventional view generation. In *Proceedings of the ACM on Web Conference 2024*, pages 1024–1034, 2024. [2](#)
- [36] Guangyue Xu, Parisa Kordjamshidi, and Joyce Chai. Prompting large pre-trained vision-language models for compositional concept learning. *arXiv preprint arXiv:2211.05077*, 2022. [1](#), [2](#)
- [37] Guangyue Xu, Joyce Chai, and Parisa Kordjamshidi. Gipcol: Graph-injected soft prompting for compositional zero-shot learning. In *Proceedings of the IEEE/CVF Winter Conference on Applications of Computer Vision*, pages 5774–5783, 2024. [1](#), [2](#)
- [38] Aron Yu and Kristen Grauman. Fine-grained visual comparisons with local learning. In *Proceedings of the IEEE conference on computer vision and pattern recognition*, pages 192–199, 2014. [6](#)
- [39] Kaiyang Zhou, Jingkang Yang, Chen Change Loy, and Ziwei Liu. Learning to prompt for vision-language models. *International Journal of Computer Vision*, pages 2337–2348, 2022. [3](#), [6](#), [7](#)